ACI STRUCTURAL JOURNAL TECHNICAL PAPER

Title No. 116-S79

Progressive Collapse-Resisting Mechanisms of Planar Prestressed Concrete Frame

by Kai Qian, Xi-De Zhang, Feng Fu, and Bing Li

This paper presents the behavior of six tests of planar prestressed concrete frames under the loss of a middle column. The six tests consist of two non-prestressed reinforced concrete (RC) specimens and four prestressed concrete (PC) specimens with bonded post-tensioning tendons (BPT). The structural response of the specimens with different flexural reinforcement ratio, span-depth ratio, and effective prestress level has been reported. In addition, the impact of parabolic BPT on the behavior of RC frames to resist progressive collapse is also evaluated. Experimental results indicated that the BPT cannot only increase the initial stiffness and yielding load of the RC counterparts, but also increase the ultimate load capacity in the catenary action stage. Moreover, it will impact the load-resisting mechanisms and the failure modes. Contrary to the commonly accepted sequential mobilization of compressive arch action and catenary action to resist progressive collapse of RC frames, no effective compressive arch action is developed in PC frames to mitigate progressive collapse risk. Based on experimental observations, it is found that higher effective prestress in BPT results in enhanced initial stiffness and yielding load but less deformation capacity and ultimate load capacity. It is also found that higher non-prestressed flexural tensile reinforcement ratio could improve the behavior of PC specimens to resist progressive collapse.

Keywords: bonded; catenary action; compressive arch action; mechanism; post-tensioning tendon; prestressed concrete; progressive collapse.

INTRODUCTION

Progressive collapse is defined as "the spread of an initial local failure from element to element, which eventually results in the collapse of an entire structure or a disproportionately large part of it."[1] As the accidents or terrorist attacks are unpredictable, conventional civil structures cannot be risk-free. Thus, one of the most popular topics in structural engineering in the last decade is evaluating the behavior and load-resisting mechanism of different types of building structures to mitigate progressive collapse risk. Currently, the commonly used method to evaluate the progressive collapse resistance of structures is based on the remaining structures following initial local failure, such as the loss of a load-bearing column or partial walls.[2-4] The alternate load path method is popular in progressive collapse design.[5-9] Based on the alternate load path method, a number of tests[2-11] have been carried out. All foregoing test results[2-11] demonstrated that considerable compressive arch action could enhance the yielding load capacity of reinforced concrete (RC) beams in relatively small deformation stage, while catenary action could develop in beam longitudinal reinforcements in large deformation stage. These tests are focused on RC frames and thus, their conclusions may not be suitable for designing of prestressed concrete (PC) frames to mitigate progressive collapse effectively. As is well known nowadays, the PC technique is frequently used in commercial buildings with long spans. Parabolic tendons with drape are commonly installed in continuous beams to apply pre-compression forces in the expected tensile zone, as shown in Fig. 1(a). However, bending moment reversal will occur in the beams after removal of the middle column, such as the initial hogging moment in the beam end at the location of the middle column changes to sagging moment after removal of the column, as shown in Fig. 1(b). If a middle column is removed accidentally, the profile of tendons will differ with the bending moment distribution along the beams. It is well known that PC frames are shallower in depth than their RC counterparts with the same span and loading conditions. Thus, PC frames may have a higher possibility of triggering progressive collapse when the profile of prestressing tendons deviate its design purpose after accidental removal of the columns. Therefore, it is imperative to carry out the investigations to capture the behavior of PC frames under the removal of a middle column. However, limited studies, especially experimental tests, have been conducted on the capacity of PC frames to mitigate progressive collapse.

The behavior of PC frames with unbonded post-tensioning (UPT) tendons was investigated by Qian et al.[12] It is well known that unbonded tendons transfer the force to the concrete via the end anchors and the profile of tendons. However, the force of bonded tendons can be transferred to the concrete through the bond between the tendons and concrete. Thus, PC frames with bonded tendons may behave quite differently from unbonded tendons.[13] Therefore, the previous work of Qian et al.[12] has been extended to carry out a program of tests on PC beam-column subassemblages with bonded post-tensioning tendons (BPT), which will be presented in this paper.

RESEARCH SIGNIFICANCE

The stress profile of tendons may differ with bending moment distribution after removal of a middle column, which may result in possible collapse of a PC frame. To quantify the possible load-resisting mechanisms of PC frames subjected to a middle column missing scenario, a series of four PC beam-column subassemblages with BPT

ACI Structural Journal, V. 116, No. 4, July 2019.

MS No. S-2017-431.R1, doi: 10.14359/51715567, was received July 22, 2018, and reviewed under Institute publication policies.

are tested in this study. By comparing to conventional RC subassemblages and PC subassemblages with UPT, the effects on BPT could be evaluated quantitatively. Due to no special provisions in existing guidelines (GSA[14] and DoD[15]) for mitigating the progressive collapse risk of PC frames, the test results may provide necessary research outcomes to fill the gap. Moreover, this research extends the availability of benchmarking data for the development of reliable analytical or numerical models, as limited test data are available in literature.

EXPERIMENTAL PROGRAM

Test specimens

Six specimens are designed and constructed to investigate the performance of PC beam-column sub-assemblages with BPT to resist progressive collapse caused by the loss of a middle column due to blast or vehicular impact. These six specimens include four PC beam-column subassemblages (PCSL-0.6, PCSL-0.75, PCSH-0.6, and PCLL-0.6) and two non-prestressed RC counterparts (RCSL and RCLL). For example, the designation of PCSL-0.6 represents a PC specimen with short span (span-depth ratio of 12), a low amount of non-prestressed reinforcement, and effective prestress (f_{pe}) of $0.6f_{pu}$, where f_{pu} is the ultimate strength of the tendon. Similarly, the designation of RCSL represents a non-prestressed RC specimen with short span and low longitudinal reinforcement ratio. Table 1 gives the designation and characteristics of each specimen. The specimens are one-half scaled due to facility capacity in laboratory. The prototype frame of the specimens is located at the middle of a perimeter frame of a six-story office building, which is 4.2 and 3.3 m (13.8 and 10.8 ft) tall in the first and upper story, respectively. The design span is 6 and 7 m (19.7 and 22.9 ft) for prototype frame with short and long span, respectively. The RC detail of the specimens follow the seismic design requirements in accordance with ACI 318-14[16] and are assumed to be located on a D class site (stiff soil profile) where the design spectral response acceleration parameters, S_{DS} and S_{D1}, are 0.45 and 0.30, respectively. The live load (LL) is assumed to be 2.0 kPa while the dead load (DL) including the self-weight is assumed to be 3.75 kPa. As shown in Fig. 2, each specimen comprises of two side columns, one middle column, and two beams. All specimens are half-scaled due to capacity limits of the test facilities. The cross section of beam and middle column are 150 x 250 mm (2.9 x 9.8 in.) and 250 x 250 mm (9.8 x 9.8 in.), respectively. However, the size of side column is enlarged to 400 x 400 mm (15.7 x 15.7 in.) for applying fixed boundary conditions well. For Specimen PCSL-0.6, beam non-prestressed reinforcements of 3T10 are installed in both top and bottom layer, which corresponds to a reinforcement ratio of 0.7%. The reinforcements are placed in the beam continuously. T10 and R6 herein represent deformed reinforcement with a diameter of 10 mm (0.4 in.) and plain reinforcement with a diameter of 6 mm (0.2 in.), respectively. As shown in the figure, a plastic duct with internal diameter of 32 mm (1.3 in.) is installed with parabolic profile before casting. After the specimen is erected in the setup, a tendon with a nominal diameter of 12.7 mm (0.5 in.) is threaded through the duct and jacked to target effective prestress $0.6f_{pu}$. Following that, grouting is conducted immediately. To ensure effective bonding between BPT and concrete, each specimen is tested after grouting over least 3 days. The true effective prestress of BPT deducting the prestress loss are measured and tabulated in Table 1. The tendon is twisted by seven high-strength wires with a nominal area of 98 mm^2 (0.2 in^2.). The parabolic profile of the tendon is following Eq. (1) and (2).

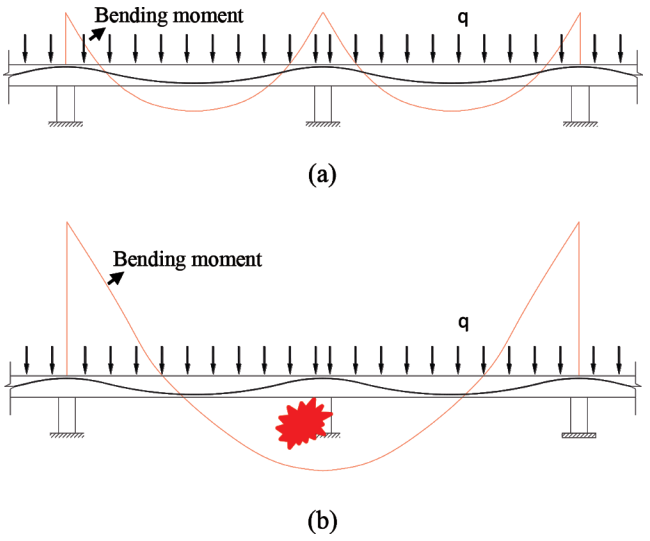

Fig. 1—Bending moment of PC sub-frame: (a) before removal of middle column; and (b) after removal of middle column.

$$y_1 = 0.12x_1^2 \quad (1)$$

Table 1—Specimen properties

Test ID	Beam clear span, mm (in.)	Diameter of post-tensioning strands, mm (in.)	Effective prestress	Effective prestress after loss	Top (bottom) beam longitudinal reinforcing bar ratio ρ	Axial force in center column, kN (kip)
RCSL	2750 (108.3)	N/A	N/A	N/A	0.7% (0.7%)	–25 (–5.6)
RCLL	3300 (129.9)	N/A	N/A	N/A	0.7% (0.7%)	–30 (–6.7)
PCSL-0.6	2750 (108.3)	12.7 (0.5)	$0.6f_{pu}$	$0.53f_{pu}$	0.7% (0.7%)	–25 (–5.6)
PCSL-0.75	2750 (108.3)	12.7 (0.5)	$0.75f_{pu}$	$0.71f_{pu}$	0.7% (0.7%)	–25 (–5.6)
PCSH-0.6	2750 (108.3)	12.7 (0.5)	$0.6f_{pu}$	$0.54f_{pu}$	1.0% (1.0%)	–25 (–5.6)
PCLL-0.6	3300 (129.9)	12.7 (0.5)	$0.6f_{pu}$	$0.55f_{pu}$	0.7% (0.7%)	–30 (–6.7)

Notes: Reinforcement ratios were determined using equation $\rho = A_s/bd_0$, in which b and d_0 represent width and effective depth of beam cross sections; f_{pu} is ultimate strength of strands.

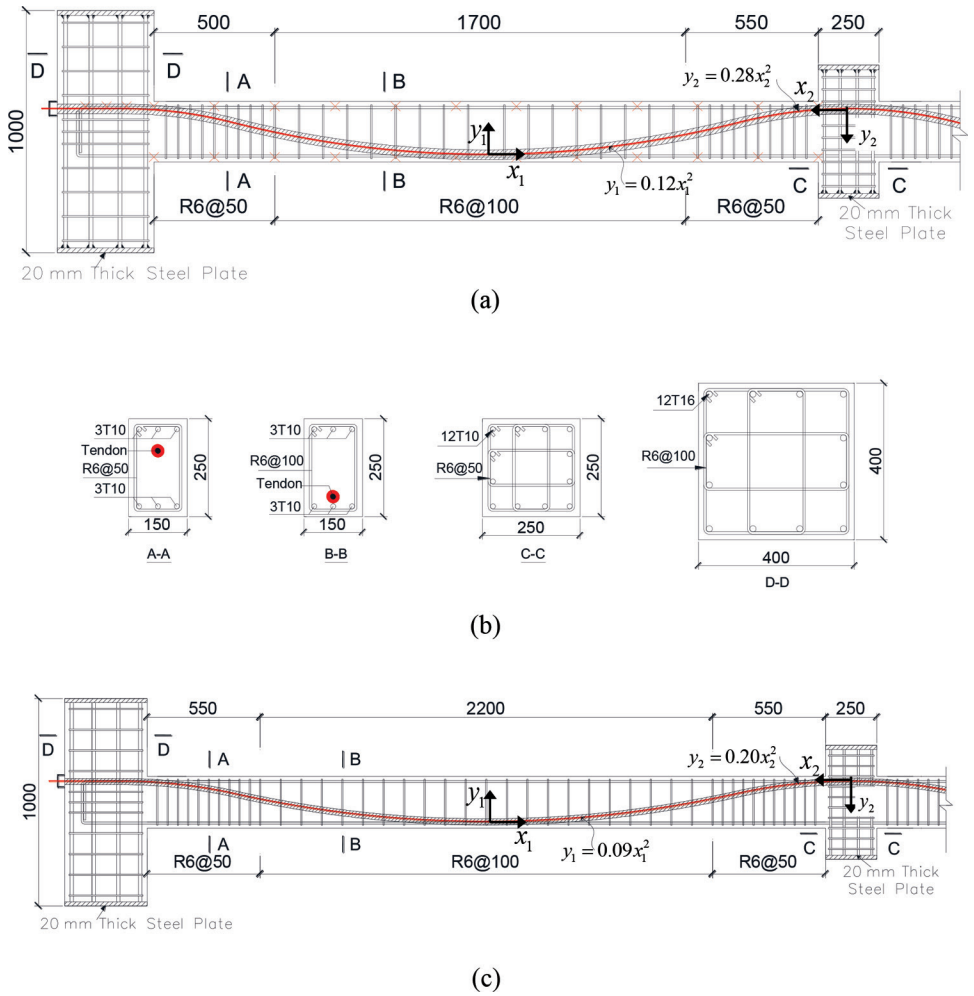

Fig. 2—Dimensions and reinforcement details: (a) Specimen PCSL-06; (b) cross sections; and (c) Specimen PCLL-0.6.

$$y_2 = 0.28x_2^2 \quad (2)$$

where y_1 is the vertical coordinate of the tendon from the origin in the middle of the beam; x_1 is the horizontal coordinate of the tendon from the origin in the middle of the beam; y_2 is the vertical coordinate of the tendon from the origin in the middle of the center column; and x_2 is the horizontal coordinate of the tendon from the origin in the middle of the center column.

PCSL-0.75 has identical dimensions and reinforcement details as PCSL-0.6 but higher designated effective prestress $0.75f_{pu}$. Comparing to PCSL-0.6, PCSH-0.6 has higher non-prestressed reinforcement ratio. In PCSH-0.6, the top and bottom beam longitudinal reinforcement are 3T12 in accordance with reinforcement ratio of 1.0%. For PCLL-0.6, it has similar cross section and reinforcement details as PCSL-0.6. However, it has a longer design span of 3500 mm (137.8 in.) and larger span-depth ratio of 14, as shown in Fig. 2(c). For easy comparison, two non-prestressed RC specimens (RCSL and RCLL) without BPT are also cast and tested. Specimens RCSL and RCLL have similar dimensions and reinforcement details as the corresponding PC Specimens PCSL-0.6 and PCLL-0.6, respectively.

Based on compressive cylindrical tests, the measured concrete compressive strength of RCSL, RCLL, PCSL-0.6, PCSL-0.75, PCSH-0.6, and PCLL-0.6 are 44, 44, 45, 44, 45, and 43 MPa (6, 6, 6, 6, 7, and 6 kip), respectively. Furthermore, based on tensile splitting tests, the tensile strength of the concrete of RCSL, RCLL, PCSL-0.6, PCSL-0.75, PCSH-0.6, and PCLL-0.6 are 3.1, 3.3, 3.0, 3.5, 3.1, and 3.4 MPa (0.4, 0.5, 0.4, 0.5, 0.4, and 0.5 kip), respectively. The properties of reinforcements and strands are tabulated in Table 2.

Table 2—Material properties of reinforcement and unbonded post-tensioning strands

Items		Nominal diameter, mm (in.)	Yield strength, MPa (ksi)	Ultimate strength, MPa (ksi)	Elongation, %
Transverse reinforcement	R6	6 (0.24)	372 (54)	510 (74)	19.5
Longitudinal reinforcements	T10	10 (0.39)	455 (66)	635 (92)	22.8
Post-tensioning strands		12.7 (0.5)	1650 (239)	1860 (270)	6.1

Notes: R6 represents plain bar of with diameter of 6 mm (0.24 in.); T10 represents deformed reinforcing bar with diameter of 10 mm (0.39 in.).

Test setup and instrumentation

Similar to previous tests,[2-5] as shown in Fig. 3, the side column is substituted with fixed boundary conditions by

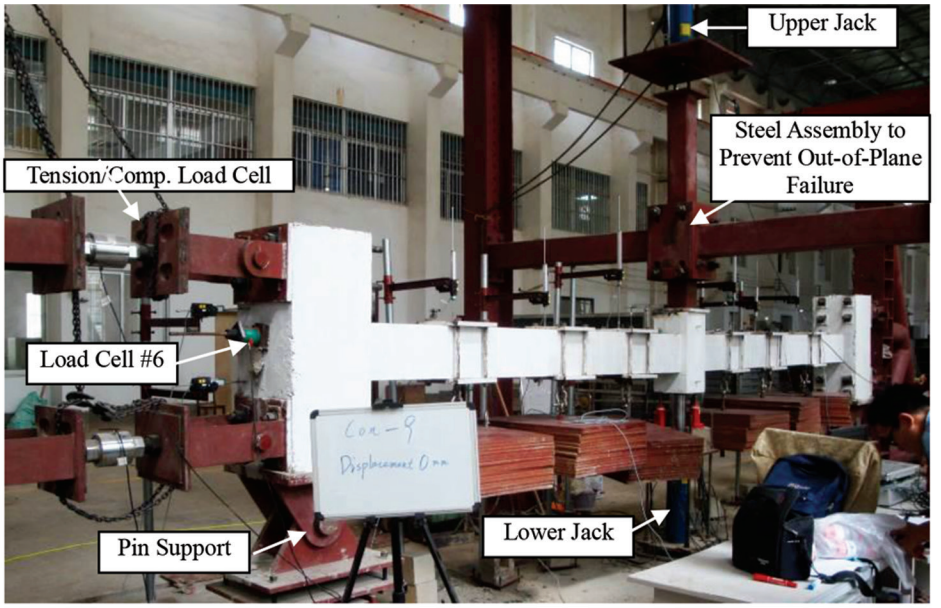

(a)

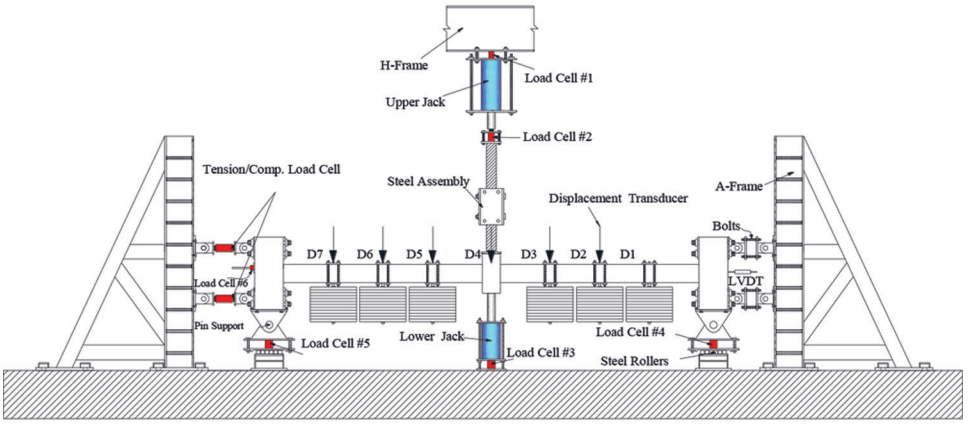

(b)

Fig. 3—Test setup and instrumentation layout of tests: (a) setup; and (b) instrumentation layout.

two horizontal constraints and a pin support. To eliminate the redundant horizontal constraints from the pin support, a series of steel rollers are mounted below it. A hydraulic jack (lower jack) is installed below the middle column stub to release of the axial force manually. The stroke of the jack is initially protruded out to touch the bottom of the middle column stub for simulation of the ground middle column intact. Then, six steel weight assemblages with weight of 5000 kg (11.0 klb) are hung below the beams to simulate the design service load (DL + LL). Once the weights are hung completely and the instrumentations are ready to record data, the stroke of the lower jack is retracted gradually to release its axial force slowly. If the specimen can stabilize after the stroke of the lower jack detaches from the bottom of the middle column stub completely, the stroke of the upper jack begins to protrude out to apply additional concentrated force on the middle column until collapse. To eliminate the out-of-plane failure of the two-dimensional (2-D) beam-column sub-assemblages, a specially designed steel assembly is installed underneath the upper jack. The steel assembly consists of a steel box and several steel pins to only allow vertical movement of the middle column but constrains its rotation and horizontal movements. A series of displacement transducers and load cells are installed to monitor the behavior of the specimens. As shown in Fig. 3(b), load cell #3 is used to measure the axial force in the lower jack. Load cells #1 and #2 are used to measure the applied additional concentrated force from upper jack. Moreover, the vertical load redistribution is measured by the load cells #4 and #5. To monitor the variation of prestressing force in the tendon, load cell #6 is installed at the jacking end. Tension/compression load cells are installed in the horizontal constraints to measure the horizontal reaction applied on the side columns. Displacement transducers D1 to D7 are installed to measure the variation of the deformation shape of the beam. Before casting, strain gauges are installed in the non-prestressed reinforcement and tendons to monitor the local behavior of the specimens.

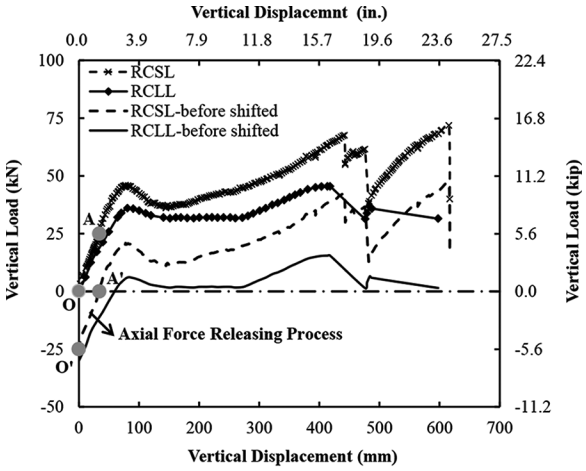

(a)

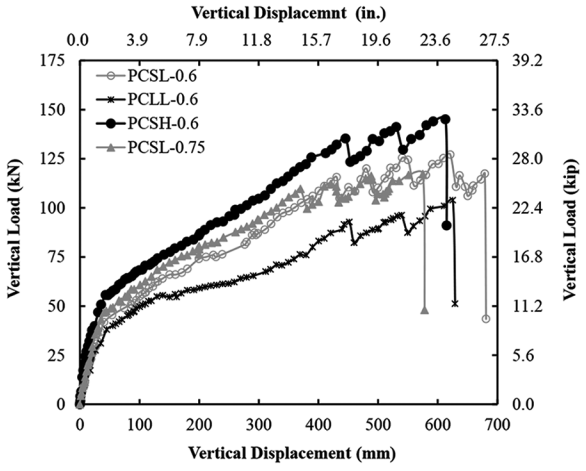

(b)

Fig. 4—Load-displacement history: (a) RC specimens; and (b) PC specimens.

TEST RESULTS

Global behavior

RC specimens—For RCSL, as previously mentioned, first, the lower jack protruded out to simulate the middle column intact. Then, six steel assemblies with total weights of 5000 kg (11.0 klb) are hung below the beams symmetrically. Thus, the vertical reaction force of –25 kN (–5.6 kip) is measured by the load cell #3 after the weights are hung completely. As shown in Fig. 4(a), the stage O′A′ represents the phase of axial force releasing in the lower jack. It can be seen that the frame structure is still within elastic range when point A′ is reached, which corresponds to a vertical displacement of 34 mm (1.3 in.). Due to bending moment reversal, the cracks in the beam end vicinity of the middle column (BEVM) form in the lower part of the section. After that, additional load is applied gradually from the upper jack until the specimen collapses. To facilitate the comparison of the performance, the load-displacement curves are shifted from [0, –25 kN (–5.6 kip)] to origin (0, 0). Take Specimen RCSL as an example—the stage O′A′ is shifted to OA. The load-displacement relationship of remaining specimens shown in the figure is after shifting. The critical values described as follows and listed in Table 3 are also picked from the shifted curves. From the shifted curve, when the vertical displacement reached 40 mm (1.6 in.), plastic hinges are formed in the beam. Further increasing the vertical displacement, the load resistance keeps increasing. This is attributed to compressive arch action developed in the beams, as shown in Fig. 5(a). When the beam ends have sufficient horizontal constraints, the developed compressive struts could distribute partial of the vertical load to the side column directly. The first peak load of the specimen is measured to 44 kN (9.9 kip) at a vertical displacement of 67 mm (2.6 in.). The load-resisting capacity began to decrease after this loading stage and severe concrete crushing occurred in the compressive zone. The re-ascending of the load-displacement curve is observed when the vertical displacement is beyond 172 mm (6.8 in.). The re-ascending is attributed into catenary action developed in beam longitudinal reinforcements (refer to Fig. 6(a)), although the concrete crushing and flexural cracks are very severe in this stage. Even though reinforcing bar fracture subsequently occurred in the beam ends, the load resistance continues increasing until the vertical displacement reached 598 mm (23.5 in.). At this stage, the ultimate load capacity of 68 kN (15.3 in.) is measured and the load resistance suddenly drops due to reinforcing bar fracture occurred in both beam ends near to the side column (BENS). The failure mode of the specimen is illustrated in Fig. 7(a). As shown in the figure, reinforcing bar fracture only occurs in the BENS. The two-span beam is deformed as parabolic curve and thus, curved catenary action is developed.

For Specimen RCLL, as it has much larger span-depth ratio, heavier steel weights of 6000 kg (13.2 klb) are designed. Thus, it results in larger initial axial force of –30 kN (6.7 kip) in the lower jack. As shown in the shifted curve, plastic hinges form in the beam when the vertical load reached 25 kN (5.6 kip), which means that the yielding load of this specimen is less than the initial axial force. If no other load-resisting mechanisms could be employed to resist the vertical load, the specimen would have collapsed during the phase of axial force releasing. Fortunately, the first peak load of 36 kN (8.1 kip) is achieved in this specimen due to compressive arch action developed in beams, which is greater than its initial axial force (30 kN [6.7 kip]). After that, the load resistance begins to decrease due to concrete crushing. When the vertical displacement reached 120 mm (4.7 in.), the displacement suddenly increased to 273 mm (10.7 in.) caused by the compressive arch action vanished, which result in the load resisting capacity less than the force transferred from the hung steel weights. However, the collapse is prevented at a vertical displacement of 273 mm (10.7 in.) due to the additional load-resistance from the catenary action. Thus, the response of this specimen demonstrated that the compressive arch action is the frontier of the defense while the catenary action is the second one. The failure mode of this specimen is shown in Fig. 7(b). Similar to RCSL, reinforcing bar fracture is only observed in BENS and the beams are deformed curved.

PC specimens—PCSL-0.6 has BPT with designed and true effective prestress of $0.6f_{pu}$ and $0.53f_{pu}$, respectively. Similar to RCSL, the initial axial force in the lower jack is

Table 3—Test results

Specimen ID	Critical displacements, mm (in.)				Critical loads, kN (kip)			MHTF kN (kip)	MPF kN (kip)
	RAF	YL	FPL	UL	YL	FPL	UL		
RCSL	34 (1.3)	40 (1.6)	67 (2.6)	598 (23.5)	32 (7.2)	44 (9.9)	68 (15.3)	153 (34.3)	N/A
RCLL	59 (2.3)	46 (1.8)	80 (3.1)	413 (16.3)	25 (5.6)	36 (8.1)	45 (10.1)	135 (30.3)	N/A
PCSL-0.6	20 (0.8)	41 (1.6)	N/A	621 (24.4)	42 (9.4)	N/A	127 (28.5)	291 (65.4)	192 (43.1)
PCSH-0.6	14 (0.6)	43 (1.7)	N/A	613 (24.1)	55 (12.3)	N/A	145 (32.6)	321 (72.1)	186 (41.8)
PCSL-0.75	19 (0.7)	40 (1.6)	N/A	575 (22.6)	46 (10.3)	N/A	117 (26.3)	265 (59.6)	187 (42.0)
PCLL-0.6	33 (1.3)	45 (1.9)	N/A	625 (24.6)	37 (8.5)	N/A	104 (23.4)	280 (62.9)	182 (40.9)

Notes: RAF represents releasing axial force completely; YL means yielding load capacity; FPL represents first peak load; UL represents ultimate load capacity; MHTF means maximum horizontal tensile force; MPF represents maximum prestressing force.

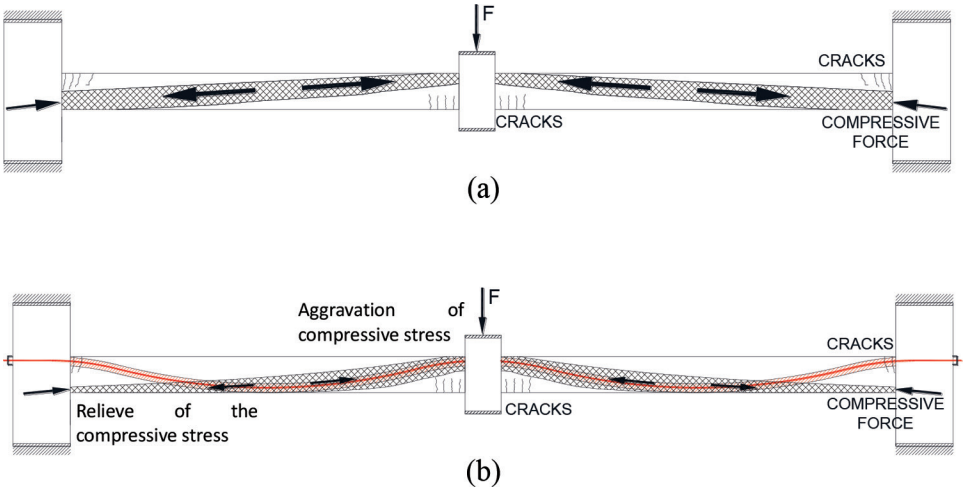

Fig. 5—Schematic of compressive arch action: (a) RC specimen; and (b) PC specimen.

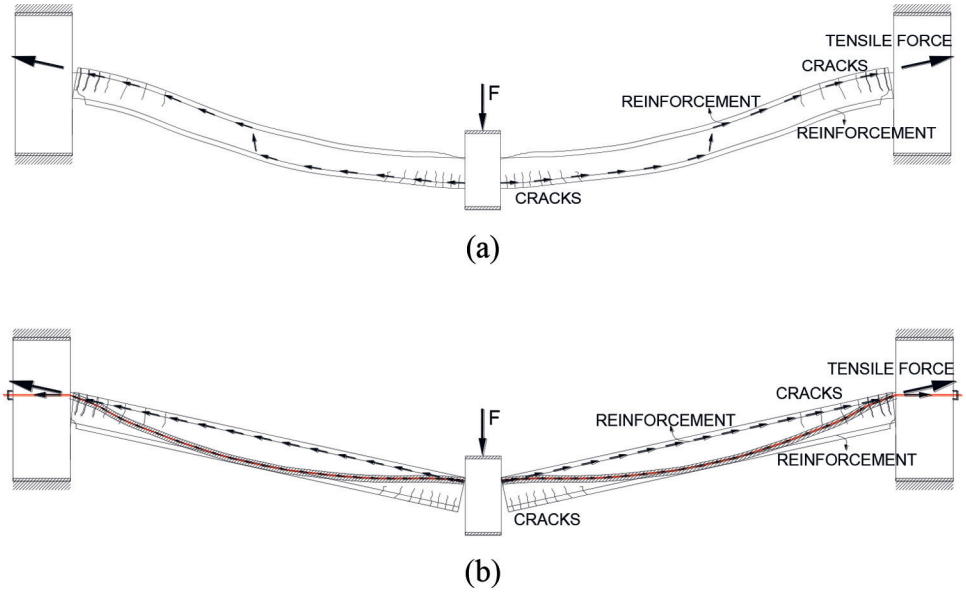

Fig. 6—Schematic of catenary action: (a) RC specimen; and (b) PC specimen.

approximately –25 kN (–5.6 kip) after the weight of 5000 kg (11.0 klb) is fully hung. Different from RCSL, no cracks are observed in the beams when the weights are applied. As shown in Fig. 4(b), the yielding load of 42 kN (9.4 kip), which is 131% of RCSL, is obtained at a vertical displacement of 41 mm (1.6 in.). At this stage, the flexural cracks at the BEVM are wider than that at the BENS, which is quite different with that in RCSL. Additionally, as the load resistance keeps increasing with further increase of the vertical displacement, the value of first peak load is hard to mark. The discussion of the load-resisting mechanism in the following section will reveal that less compressive arch action is developed in PC beams but the stretching of the tendon will provide additional resistance. When the displacement

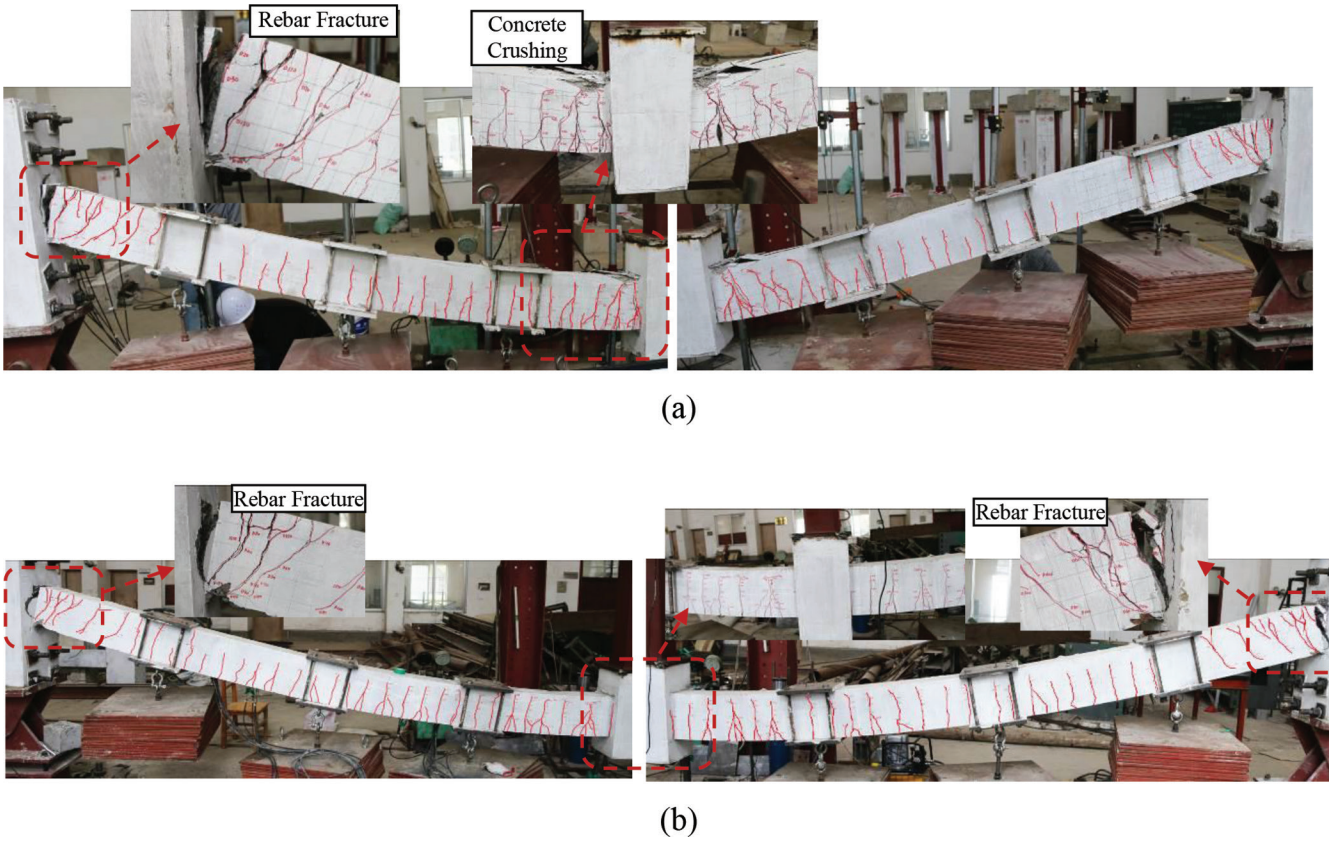

Fig. 7—Failure mode of controlled RC specimens: (a) RCSL; and (b) RCLL.

reached 480 mm (18.9 in.), reinforcing bar fracture first occurred in the left BEVM. With the further increase of the displacement to 560 and 621 mm (22.0 and 24.4 in.), reinforcing bar fractures are also observed in the BENS. The ultimate load capacity in catenary action stage is measured to 127 kN (28.5 kip), which is 187% of that of RCSL. Thus, BPT could increase the ultimate load capacity significantly. The test stopped at a vertical displacement of 679 mm (26.7 in.) due to anchor slip occurred in the jacking end. The failure mode of this specimen is shown in Fig. 8. Different to RCSL, the PC beams with BPT deformed straightly and the widest crack is formed in the BEVM. Moreover, comparing to RCSL, the crack width in the BENS is much thinner.

Similar to RCLL, PCLL-0.6 has a span-depth ratio of 14 and thus, the initial axial force is –30 kN (6.7 kip). The true effective prestress of the tendon is $0.55f_{pu}$ due to prestress loss. The measured vertical displacement is 33 mm (1.3 in.) when the axial force is fully released. The yielding load of this specimen is 37 kN (8.5 kip), which is 148% of that of RCLL, at a vertical displacement of 45 mm (1.8 in.). Thus, comparing to PCSL-0.6, BPT is more effective for upgrading the yielding load of RCLL. Similar to PCSL-0.6, it is hard to mark the first peak load in the curve, as the load-displacement curve also keeps increasing with increase of the vertical displacement. Reinforcing bar fracture is first observed in the BEVM at a vertical displacement of 452 mm (17.8 in.). When the vertical displacement reached 550 mm (21.7 in.), reinforcing bar fracture also occurred in the left BENS. The failure mode of this specimen is illustrated in Fig. 9. Similar to PCSL-0.6, the beams are deformed straightly. Different to

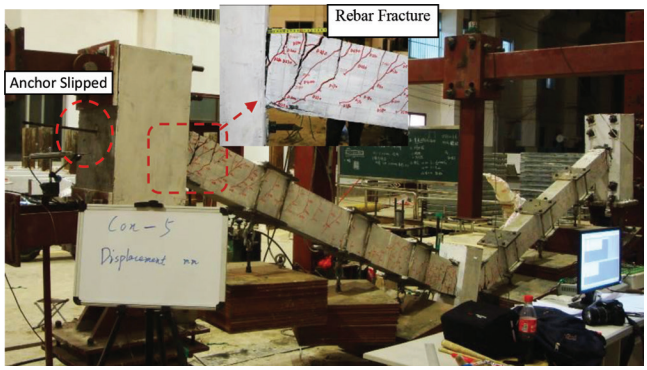

Fig. 8—Failure mode of PC specimen PCSL-0.6.

RCLL, more severe damage is occurred in the BEVM than that in BENS.

Comparing to PCSL-0.6, PCSH-0.6 has higher beam longitudinal reinforcement ratio of 1.0%. The vertical displacement is 14 mm (0.6 in.) when the initial axial force in the lower jack is released completely. The yielding load of 55 kN (12.3 kip) is achieved at a vertical displacement of 43 mm (1.7 in.). Thus, comparing to PCSL-0.6, PCSH-0.6 achieved much higher initial stiffness and yielding load. Similar to foregoing PC specimens, the load resistance increases with further increasing the displacement, although concrete crushing and wide cracks are accompanied. The load resistance first dropped when the vertical displacement reached 445 mm (17.5 in.) due to reinforcing bar fracture occurring in the right BEVM. Reinforcing bar fracture is also observed in the left BENS at a displacement of 613 mm

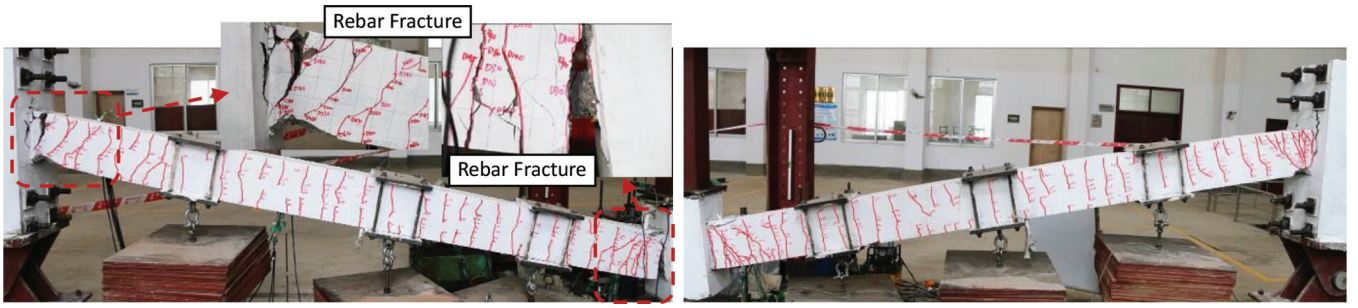

Fig. 9—Failure mode of PC specimen PCLL-0.6.

Fig. 10—Failure mode of PC specimen PCSH-0.6.

Fig. 11—Failure mode of PC specimen PCSL-0.75.

(24.1 in.). The measured ultimate load capacity is 145 kN (32.6 kip), which is approximately 114% of that in PCSL-0.6.

Comparing to PCSL-0.6, PCSL-0.75 has larger designed effective prestress of $0.75f_{pu}$ and the true effective prestress of $0.71f_{pu}$. Comparing to other PC specimens, the camber of 3 mm (0.1 in.) in the middle span of the beam is measured before applying the weights. The vertical displacement is measured to be 19 mm (0.7 in.) after completely releasing of the axial force in the lower jack. Moreover, the yielding load of 46 kN (10.3 kip) is measured at a vertical displacement of 40 mm (1.6 in.). Thus, higher initial effective prestress will increase the initial stiffness slightly. The reinforcing bar fracture first occurred in the right BENM at a vertical displacement of 361 mm (14.2 in.), which is much earlier than that in PCSL-0.6. Subsequently, it occurred in both BENS at displacements of 490 and 524 mm (19.3 and 20.6 in.), respectively. The specimen stopped at a vertical displacement of 575 mm (22.6 in.) due to anchor slip occurring in the jacking point, similar to PCSL-0.6. The failure modes of PCSH-0.6 and PCSL-0.75 are shown in Fig. 10 and 11, respectively.

Horizontal reaction

As shown in Fig. 12, for RCSL, considerable compressive force is measured at the lower roller initially. It begins to decrease after vertical displacement reached 100.6 mm (4.0 in.) due to concrete crushing. Tensile force is measured in the lower roller when the vertical displacement reached 487.5 mm (19.2 in.). However, the upper roller consistently measured tensile force during the test. Thus, the total compressive force in relatively small displacement stage is mainly attributed to the lower roller, while the total tensile force in large displacement stage is attributed to both rollers. However, for PCSL-0.6, much larger tensile force is measured in the upper roller from the beginning of the test due to substantial tensile force from BPT. Moreover, although compressive force is also measured in the lower roller, the maximum compressive force is –65.6 kN (–14.7 kip), which is much less than that of RCSL.

Looking at the total reaction force, similar to previous RC tests,[3-11] for RC specimens, significant compressive reaction force is initially measured in the horizontal constraints. As shown in Fig. 13, the maximum compressive reaction force of –136 and –142 kN (–30.6 and –32.0 kip) are measured in RCSL and RCLL, respectively. The compressive reac-

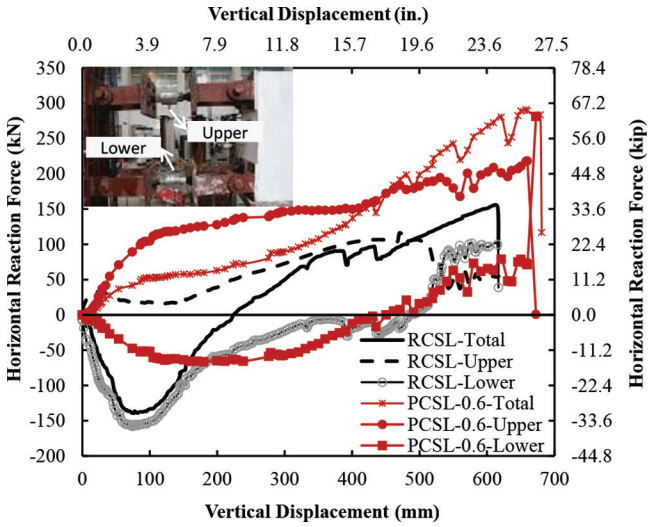

Fig. 12—Horizontal reaction force of lower and upper roller.

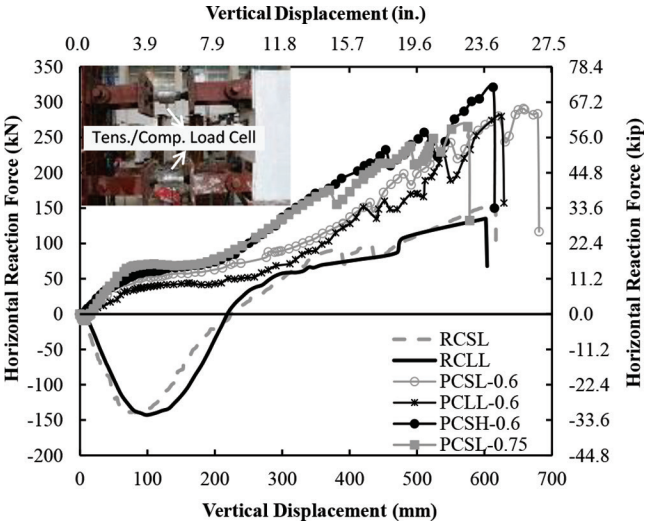

Fig. 13—Comparison of horizontal reaction force-displacement history.

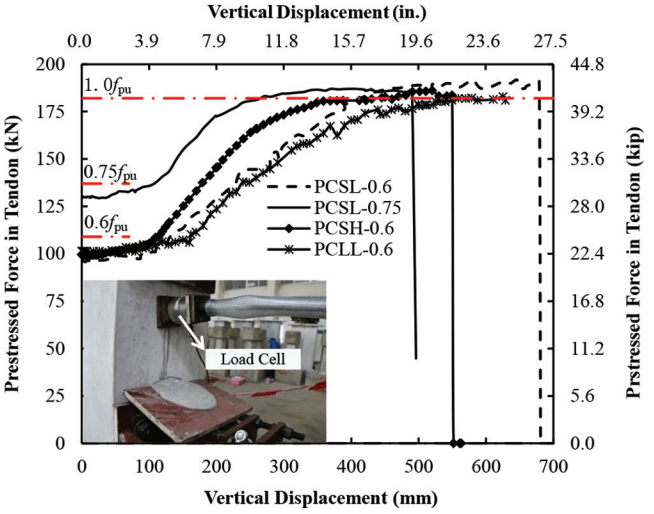

Fig. 14—Prestressed force in tendon of all specimens.

tion force began to decrease when the displacement beyond 80 mm (3.1 in.) ($0.03l_n$) and 100 mm (3.9 in.) ($0.03l_n$) for RCSL and RCLL, respectively. l_n represents the clear span of a single beam. In accordance with their load-resisting behavior, the decrease of the horizontal reaction force related to the compressive arch action vanishing and concrete crushing. When the vertical displacement went beyond 220 mm (8.7 in.) ($0.08l_n$ for RCSL and $0.07l_n$ for RCLL), tensile force is measured. The maximum horizontal tensile forces in RCSL and RCLL are 153 and 135 kN (34.3 and 30.3 kip), respectively. However, different from RCSL and RCLL and previously tested RC specimens,[3-11] for PC specimens PCSL-0.6, PCLL-0.6, PCSH-0.6, and PCSL-0.75, no compressive reaction force is observed during the test, which further confirmed less compressive arch action is developed in PC beams. As explained in Fig. 5(b), the post-tensioning tendon will aggravate the compressive stress at the BEVM but relieve the compressive stress at the BENS. Thus, no effective compressive strut is able to develop in the beams for load redistribution. However, the tensile reaction force remains constant when the vertical displacement reached 70 to 80 mm (2.8 to 3.1 in.). The re-ascending of the tensile reaction force is observed in PC specimens with short and long span at the displacements of 170 and 190 mm (6.7 and 7.5 in.), respectively. With increasing the vertical displacement, the horizontal tensile force keeps increasing. The maximum tensile reaction force measured in PCSL-0.6, PCSH-0.6, PCSL-0.75, and PCLL-0.6 is 291, 321, 265, and 280 kN (65.4, 72.1, 59.6, and 62.9 kip), respectively. The lower reaction force measured in PCSL-0.75 is due to anchor slip occurring in the jacking end at the relatively early vertical displacement of 575 mm (22.6 in.).

Prestressing force in BPT

Figure 14 presents the response of prestress force in the tendon versus the vertical displacement. As shown in the figure, the initial prestress force deducting prestress loss is 97, 100, 130, and 101 kN (21.8, 22.5, 29.2, and 22.7 kip) in PCSL-0.6, PCSH-0.6, PCSL-0.75, and PCLL-0.6, respectively. It is found that the prestress force increased slowly before the vertical displacements reached 100 and 150 mm (3.9 and 5.9 in.) for PC specimens with short and long span, respectively. Comparing the response of horizontal reaction force with prestress force in PC specimens, it is hard to explain the increase of tensile reaction force in the initial stage. It is suggested that because bonded tendons are used in this study, the prestress force measured in the jacking end could not represent the variation of the prestress force of the tendon in other places well. When the vertical displacements exceed 100 mm and 150 mm (3.9 and 5.9 in.) for PC specimens with short and long span, respectively, the increase of the prestress force is linear until yielding. Based on the test results, the maximum tensile force in the tendon of PCSL-0.6, PCSH-0.6, PCSL-0.75, and PCLL-0.6 are 192, 186, 187, and 182 kN (43.1, 41.8, 42.0, and 40.9 kip), respectively. They are related to prestress stress of $1.05f_{pu}$, $1.02f_{pu}$, $1.03f_{pu}$, and $1.0f_{pu}$, respectively.

Deformation shape of beams

Figure 15 gives the beam deformation shape of typical RC and PC specimen in accordance with critical stages: the

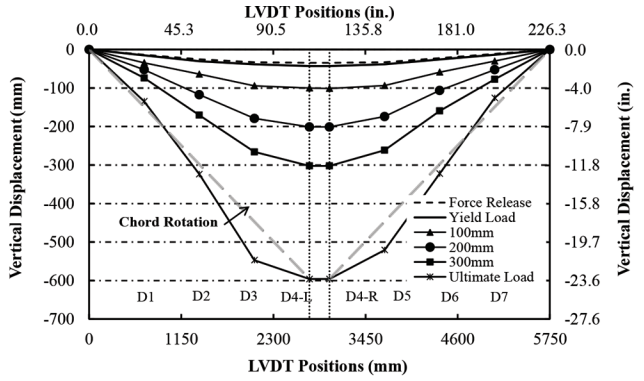

(a)

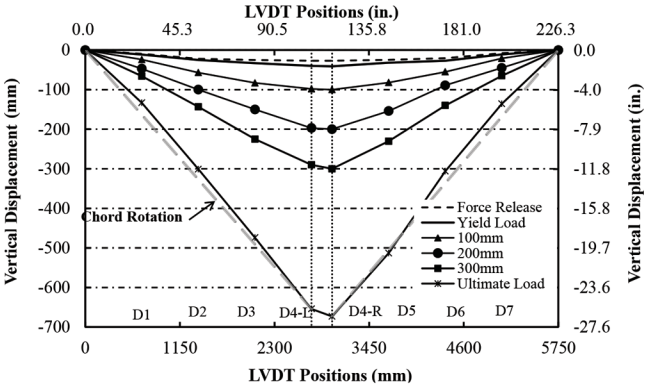

(b)

Fig. 15—Deformation shape of test specimens: (a) RCSL; and (b) PCSL-0.6.

axial force just released, yield load, first peak load, 100 mm (3.9 in.), 200 mm (7.9 in.), 300 mm (11.8 in.), and ultimate load. As shown in Fig. 15(a), for RCSL, the deformation shape of beam is curved. In the ultimate load stage, the chord rotation, which is defined as the ratio of displacement in the middle column to the clear span of the beam,[15] will slightly over-estimate the rotation of the BESC but significantly under-estimate the rotation in BEVM. This is quite different with that observed in previous tests[2,4-6] as the initial service load is well simulated in this study. For PCSL-0.6, as shown in Fig. 15(b), the beam is deformed straightly when the displacement is beyond 100 mm (3.9 in.) and severe flexural cracks are formed in the BEVM. In the ultimate load stage, the chord rotation agrees the deformation shape of the beam well, although it is originally defined for non-prestressed RC specimen in existing design guideline.[15]

Strain gauge reading

Figures 16(a) and (b) show the variation of strain results along beam top and bottom longitudinal reinforcements of PCSL-0.6, respectively. As shown in the figures, similar to non-prestressed RC specimens,[4] bending moment reversal is observed at the BEVM after releasing of the initial axial force in the lower jack. Yielding first occurred in the top reinforcement at the BENS, rather than the bottom reinforcement at the BEVM, which is quite different to the previous non-prestressed RC specimens.[4] Moreover, the compressive strain in the beam longitudinal reinforcements begins to

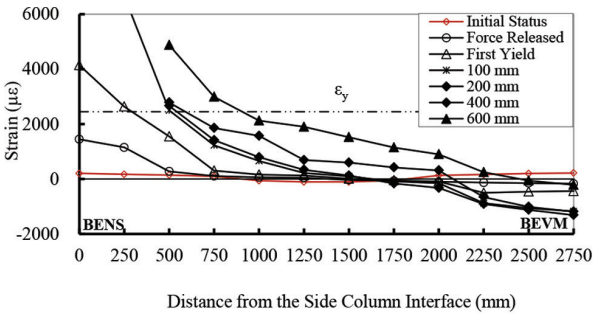

(a)

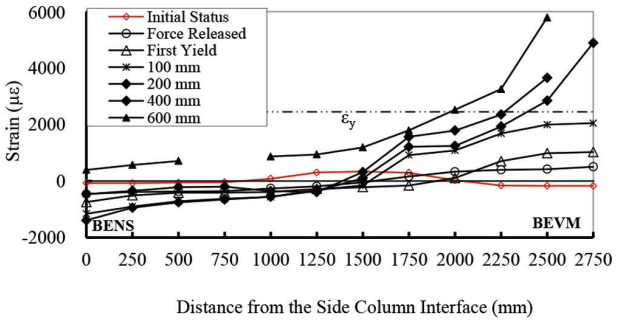

(b)

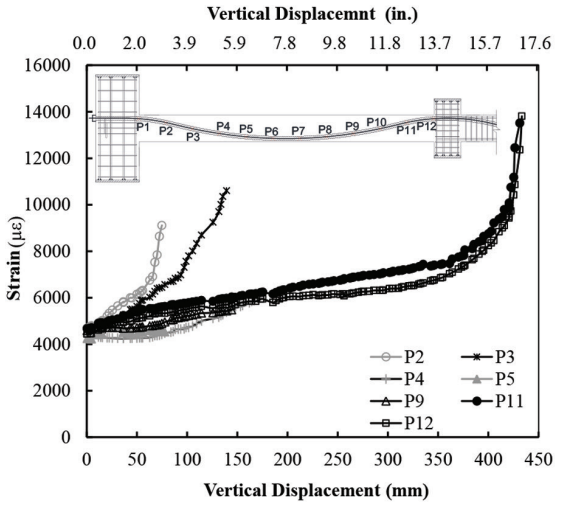

(c)

Fig. 16—Strain gauge results of PCSL-0.6: (a) top non-prestressed reinforcing bar; (b) bottom non-prestressed reinforcing bar; and (c) prestressed tendon.

decrease when the vertical displacement is beyond 400 mm (15.7 in.). When the vertical displacement reached 600 mm (23.6 in.), the bottom reinforcement is in tension across the whole span. Figure 16(c) gives the results of strain gauges attached on the post-tensioning tendons. Due to unknown reasons, part of the strain gauges were faulty before tests. As shown in the figure, initially, all strain gauges read similar values ranging from 4400 to 4600 με. When the vertical displacement increased, P2 and P3—which are near to the side column—increased their strain dramatically with high slope. However, the increase of remaining strain gauges is relatively very slow. It can be seen that P11 and P12, which

are near the BEVM, suddenly increased abruptly when the vertical displacement is beyond 400 mm (15.7 in.). Actually, as shown in Fig. 6(b), the tendon at the BEVM will become a straight line when the vertical displacement reached 400 mm (15.7 in.).

ANALYTICAL ANALYSIS AND DISCUSSIONS

Dynamic performance of tested specimens

The scenario of column missing caused by terrorist attacks is considered in this study. The most realistic setup should be designed by removal of the column suddenly. Although quasi-static pushdown test is most commonly used for evaluation of the performance of beam-column substructures mitigating progressive collapse, it is still necessary to assess the dynamic behavior of beam-column substructures. The capacity curve method, which was first proposed by Izzuddin et al.,[17] is frequently used to predict the dynamic capacity of the substructures based on the measured load-displacement curves (Tsai and Lin[18] and Qian and Li[19]). The capacity curve method is mathematically expressed as

$$P_{CC}(u_d) = \frac{1}{u_d}\int_0^{u_d} P_{NS}(u)du \tag{3}$$

where $P_{CC}(u)$ and $P_{NS}(u)$ represent the capacity function and the nonlinear static loading estimated at the displacement demand u, respectively.

Figure 17 shows the dynamic behavior of test specimens. It is found that the dynamic ultimate capacity of RCSL, RCLL, PCSL-0.6, PCSL-0.75, PCSH-0.6, and PCLL-0.6 are 46.7, 33.2, 88.0, 90.8, 103.8, and 69.2 kN (10.5, 7.5, 19.8, 20.4, 23.3, and 10.5 kip), respectively.

Decomposite resistance contribution of axial force and bending moment

For the process of releasing of axial force in the middle column, based on equilibrium and refer to Fig. 18, the bending moment (M_L^M), axial force (N_L^M), and shear force (V_L^M) at Section A-A are determined as

$$M_L^M = V_L L_L - H_t^L(\delta+0.35) - H_b^L(\delta-0.35) - G_7 \times 2.0625 - G_6 \times 1.375 - G_5 \times 0.6875 - \frac{1}{2}q \times L^2 \tag{4}$$

$$N_L^M = [(V_L - G_7 - G_6 - G_5)\tan\theta_L^M + H_L]\cos\theta_L^M \tag{5}$$

$$V_L^M = [(V_L - G_7 - G_6 - G_5) - N_L^M \sin\theta_L^M)]/\cos\theta_L^M \tag{6}$$

where V_L is the vertical reaction force measured by load cell #5 in Fig. 3(b); H_t^L and H_b^L are the horizontal reaction force from upper and lower roller, respectively; G1 to G7 are the gravitational load of single weight assembly (8.2 kN [1.8 kip]); q is assumed to be 0.001 kN/mm (0.006 kip/in.) for consideration of the self-weights of the beam; θ_L^M = arctan([D_4 – D_5]/0.6875) is based on chord rotation of the segment.

Similarly, the bending moment (M_R^M), axial force (N_R^M), and shear force (V_R^M) in the symmetric section of right beam are determined as

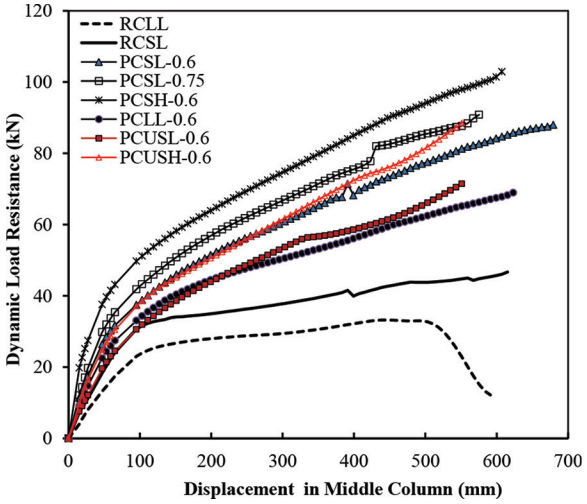

Fig. 17—Dynamic performance of specimens.

$$M_R^M = V_R L_R - H_t^R(\delta+0.35) - H_b^R(\delta-0.35) - G_1 \times 2.0625 - G_2 \times 1.375 - G_3 \times 0.6875 - \frac{1}{2}q \times L^2 \tag{7}$$

$$N_R^M = [(V_R - G_1 - G_2 - G_3)\tan\theta_R^M + H_R]\cos\theta_R^M \tag{8}$$

$$V_R^M = [(V_R - G_1 - G_2 - G_3) - N_R^M \sin\theta_R^M]/\cos\theta_R^M \tag{9}$$

where V_R is the vertical reaction force measured by load cell #4 in Fig. 3(b); H_t^R and H_b^R respectively are assumed equal to H_t^L and H_b^L, as no load cells are installed for measuring; and θ_R^M = arctan([D_4 – D_3]/0.6875) is based on chord rotation of the segment.

After that, based on the vertical force equilibrium at the middle joint, it is determined that

$$P = (N_L^M \sin\theta_L^M + V_L^M \cos\theta_L^M) + (N_R^M \sin\theta_R^M + V_R^M \cos\theta_R^M) \tag{10}$$

After rearrangement, it becomes

$$P = (N_L^M \sin\theta_L^M + N_R^M \sin\theta_R^M) + (V_L^M \cos\theta_L^M + V_R^M \cos\theta_R^M) = \sum_r^{L,R} N_r^M \sin\theta_r^M + \sum_r^{L,R} V_r^M \cos\theta_r^M \tag{11}$$

where $\sum_r^{L,R} N_r^M \sin\theta_r^M$ and $\sum_r^{L,R} V_r^M \cos\theta_r^M$ represent the resistance contribution from axial force and shear force, respectively. As the shear force could be determined by the bending moment acting on the beams, $\sum_r^{L,R} V_r^M \cos\theta_r^M$ can also be taken as the contribution from the bending moment. For the process of applying extra axial force on the middle column, the sign of the applied load and shear force will reverse. However, the equations for determination of the internal force are identical. For the sake of brevity, RCSL, PCSL-0.6, and PCSH-0.6 are selected to show the decomposition of vertical resistance.

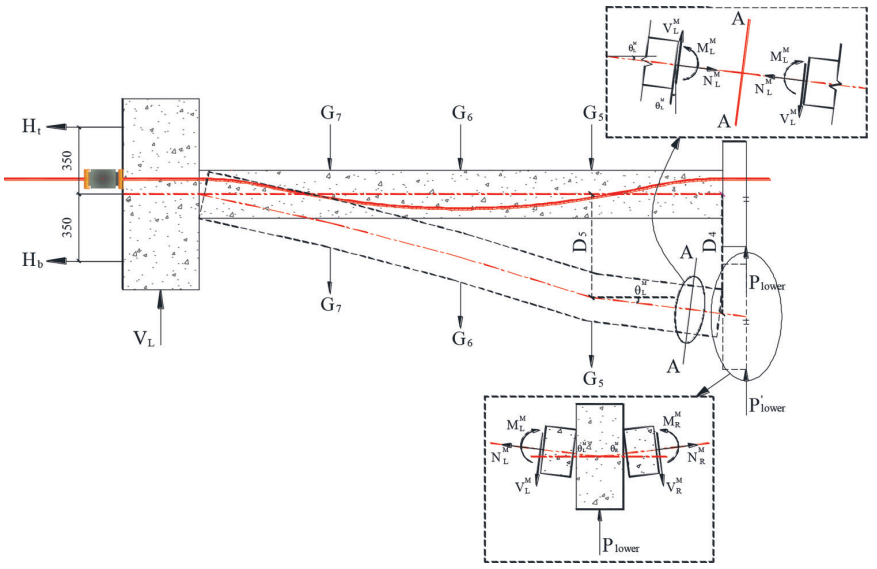

Fig. 18—Relationship of internal forces and load resistance.

As shown in Fig. 19(a), the contribution of shear force begins to decrease after crushing occurred in the beam sections. The re-ascending of the load-resisting capacity in catenary action stage is mainly due to the contribution of axial force changing from compression to tension. However, as observed in the figure, before fracture of beam longitudinal reinforcements, shear force (or flexural bending moment) could also provide considerable contribution in the stage of catenary action. Therefore, it is unrealistic to assume the load-resisting capacity of the substructures in catenary action stage purely attributed into the tension of beam longitudinal reinforcements, which is commonly accepted by previous studies.[20]

As shown in Fig. 19(b), for PCSL-0.6, the varying of the contribution of shear force is similar to RCSL. However, the contribution of axial force is quite different as the strands could provide considerable tension at the beginning of the test. If the axial force contribution is further decomposited, it is found that compression actually is also observed at the axial force component from RC beam. Moreover, the maximum compression force of 7.5 kN (1.7 kip) is measured in the axial force component from RC beam, which is similar to RCSL. As similar results are observed in PCSH-0.6, no further discussion is given for it.

Effects of span-depth ratio

As shown in Fig. 4 and Table 3, compared with RCLL, RCSL achieved greater yielding, first peak, and ultimate load by 28%, 22%, and 51%, respectively. However, for PC specimens, the yielding and ultimate load capacity of PCSL-0.6 is approximately 114% and 122% of that of PCLL-0.6. Thus, the span-depth ratio has greater effects for RC specimens than PC specimens, especially for ultimate load capacity in catenary action stage. As shown in Fig. 7, 8, and 9, for both RC and PC specimens, the span-depth ratio has little effect on their failure modes (widest flexural cracks are occurred at the beam end nearby the columns) as the span-depth ratio is 12 and 14 for specimens with short and long design span, respectively. Both span-depth ratios are large enough for flexural dominated failure in beams. Another reason is the prototype frames are seismic designed and detailed, which have high transverse reinforcement ratio in the beam ends nearby the columns and prevented the possible shear failure at the beam end due to smaller span-depth ratio.

Effects of amount of non-prestressed reinforcements

In comparison of the behavior of PCSL-0.6 and PCSH-0.6, it is found that higher non-prestress reinforcement ratio (1.0%) could increase the yielding load and ultimate load capacity by 31% and 14%, respectively. As listed in Table 3, the initial stiffness of PCSL-0.6 and PCSH-0.6 are 0.93 and 1.23 kN/mm (5.3 and 7.0 kip/in.), respectively. Thus, PCSH-0.6 increased the initial stiffness by 32%. As shown in Fig. 8 and 10, the amount of non-prestressed reinforcement ratio has little effect on the failure mode and load-resisting mechanism of PC frames to resist progressive collapse. This could be explained as the non-prestressed reinforcement ratio is 0.7% or 1.0% for PC specimens with light or heavy non-prestressed reinforcement, respectively. Similar to the earlier explanation, the relatively heavy transverse reinforcement ratio installed in the beam end nearby the column prevents the possible shear failure even relatively heavy non-prestressed reinforcement ratio is designed.

Effects of initial effective prestress

Compared to PCSL-0.6, PCSL-0.75 achieved a 10% increase of yielding load. However, PCSL-0.75 exhibited lower ultimate load capacity. This is due to anchor slip occurring in the jacking end at the displacement of 575 mm (22.6 in.), which prevented the tendon from further developing catenary action. As shown in Fig. 8 and 11, initial effective prestress has little effects on the failure mode of the specimen.

Effects of bonded post-tensioning tendons

By comparing the behavior of PCSL-0.6 with RCSL, it is found that BPT could increase the yielding and ultimate load capacity by 31% and 87%, respectively. For PCLL-0.6,

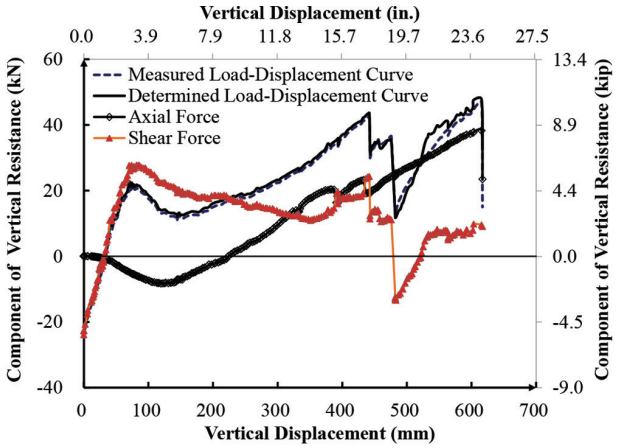

(a)

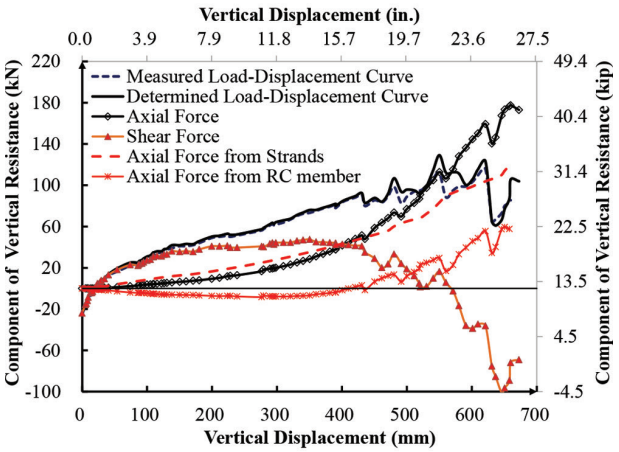

(b)

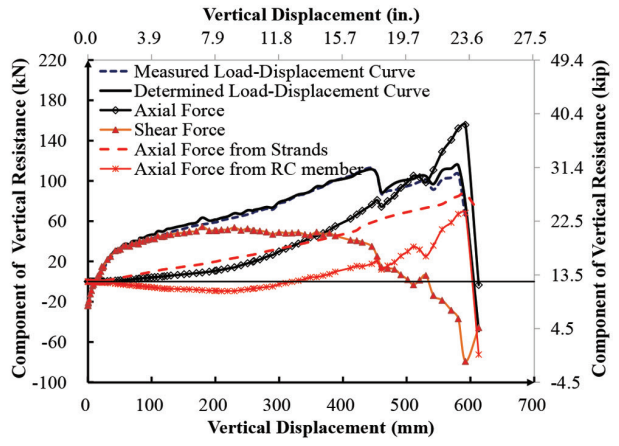

(c)

Fig. 19—Resistance contributions from axial and shear force: (a) RCSL; (b) PCSL-0.6; and (c) PCSH-0.6.

the BPT increased the yielding and ultimate load capacity of RCLL by 48% and 131%, respectively. Thus, BPT has greater impacts on behavior of specimens with larger span-depth ratio. As shown in Fig. 13, considerable compressive reaction force is developed in RC beams in the compressive

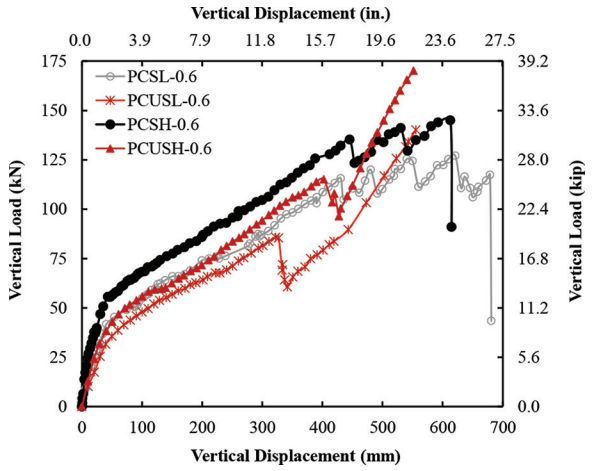

Fig. 20—Bonding effects on load-displacement curves.

arch action stage, but not PC specimens. This is because little compressive arch action can be developed in PC beams to resist progressive collapse. Comparing the failure mode of PC specimens with corresponding RC specimens, it is found that the BPT will aggravate the damage in the BEVM and relief the damage in the BENS. In PC specimens, reinforcing bar fracture is first observed in the BEVM, while no reinforcing bar fracture is observed in RC specimens, as shown in Fig. 7, 8, and 9. As shown in Fig. 6, straight catenary action and curved catenary action are developed in PC and RC specimens, respectively. Figure 20 illustrates the comparison of the load-displacement curves from PC specimens with bonded strands and counterparts with unbonded strands (PCUSL-0.6 and PCUSH-0.6). The results of PCUSL-0.6 and PCUSH-0.6 have been discussed in the authors' previous paper.[12] As shown in Fig. 20, PCUSL-0.6 and PCUSH-0.6 achieve relatively less initial stiffness and yield load comparing to PCSL-0.6 and PCSH-0.6, respectively. However, in catenary actions stage, the ultimate load capacity of PCUSL-0.6 and PCUSH-0.6 are 140 and 170 kN (31.5 and 38.2 kip), respectively. Thus, PC specimens with unbonded strands are able to mobilize larger catenary action as the stress in unbonded strands are more uniform, which prevents premature fracture of the strands in catenary action stage. Due to spacing limitations, the effects on bonding of strands on horizontal reaction force and failure modes are not discussed herein.

CONCLUSIONS

Based on the results of this experimental investigation, the following conclusions are drawn:

1. Different to conventional RC frames, post-tensioning concrete (PC) frames have few benefits from compressive arch action to prevent progressive collapse. However, the stretching of bonded post-tensioning tendons (BPT) could provide additional vertical load resistance from the beginning of the test. However, the BPT will not detriment the deformation capacity of the frames and thus, the catenary action attributed to both non-prestressed reinforcements and BPT, which could provide a reliable second defense line for progressive collapse prevention. BPT could increase the

yield load and ultimate capacity of corresponding RC counterpart by 48% and 131%, respectively.

2. Test results indicated that higher initial effective prestress in the BPT will increase the yield load capacity of the PC frame slightly, but not the ultimate load capacity. Analytical analysis and test results revealed that the ultimate load capacity of the PC frame is dependent on the amount of BPT and non-prestressed reinforcement ratio, rather than the initial effective prestress in the BPT. Inversely, the potential of earlier fracture of BPT raised by high initial effective prestress in the tendon should be given attention.

3. Based on the test results, it is found that the RCLL with larger span-depth ratio of 14 will reduce the yield load and ultimate load capacity by 22 and 34%, respectively. However, PCLL-0.6 with larger span-depth ratio of 14 only decreases the yield load and ultimate load capacity of PC frames only by 12 and 18%, respectively. Thus, the span-depth ratio has less effect on PC frames than RC frames.

4. The amount of non-prestressed reinforcement could improve the capacity of PC frames to resist progressive collapse, including yielding and ultimate load capacities. Further studies should be conducted to capture the optimal ratio of prestressed reinforcement to non-prestressed reinforcements for optimal resilience performance.

FUTURE RESEARCH

As the loss of column is instantaneous due to blast or vehicular impact, further research studies are needed on dynamic performance of prestressed concrete frames subjected to sudden column removal scenario. Moreover, more studies should be carried out that include the impact effects of disasters such as fire and blast impact or pressure.

AUTHOR BIOS

ACI member **Kai Qian** *is a Professor in the College of Civil Engineering and Architecture at Guilin University of Technology, Guilin, China. He received his MSC and PhD from Nanyang Technological University, Singapore. His research interests include reinforced concrete and prestressed concrete structures design, particularly in the area of progressive collapse and blast resistance.*

Xi-De Zhang *is a Professor in the College of Civil Engineering and Architecture at Guangxi University, Nanning, China. His research interests include reinforced concrete and composite structures design, particularly in the area of seismic resistance.*

Feng Fu *is a Lecturer in Structural Engineering, City, University of London, London, UK, and Changbai Mountain Distinguished Professor at Jilin Jianzhu University, Jilin, China. His research interests include finite element simulation on reinforced concrete and composite structures, particularly in the area of progressive collapse and blast resistance.*

ACI member **Bing Li** *is an Associate Professor in the School of Civil and Environmental Engineering at Nanyang Technological University. He received his PhD from the University of Canterbury, Christchurch, New Zealand. He is a member of ACI Committee 377, Performance-Based Structural Integrity and Resilience of Concrete Structures, and Joint ACI-ASCE Committees 352, Joints and Connections in Monolithic Concrete Structures, and 441, Reinforced Concrete Columns.*

ACKNOWLEDGMENTS

This research was supported by a research grant provided by the Natural Science Foundation of China (No. 51778153, 51568004, and 51478118). Any opinions, findings, and conclusions expressed in this paper do not necessarily reflect the view of Natural Science Foundation of China.

REFERENCES

1. ASCE/SEI 7, "Minimum Design Loads for Buildings and Other Structures," Structural Engineering Institute-American Society of Civil Engineers, Reston, VA, 2010, 424 pp.

2. Su, Y. P.; Tian, Y.; and Song, X. S., "Progressive Collapse Resistance of Axially-Restrained Frame Beams," *ACI Structural Journal*, V. 106, No. 5, Sept.-Oct. 2009, pp. 600-607.

3. Orton, S.; Jirsa, J. O.; and Bayrak, O., "Carbon Fiber-Reinforced Polymer for Continuing in Existing Reinforced Concrete Buildings Vulnerable to Collapse," *ACI Structural Journal*, V. 106, No. 5, Sept.-Oct. 2009, pp. 608-616.

4. Yu, J., and Tan, K. H., "Experimental and Numerical Investigation on Progressive Collapse Resistance of Reinforced Concrete Beam Column Sub-Assemblages," *Engineering Structures*, V. 55, 2013, pp. 90-106. doi: 10.1016/j.engstruct.2011.08.040

5. Sasani, M., and Kropelnicki, J., "Progressive Collapse Analysis of an RC Structure," *Structural Design of Tall and Special Buildings*, V. 17, No. 4, 2008, pp. 757-771. doi: 10.1002/tal.375

6. Lew, H. S.; Bao, Y. H.; Pujol, S.; and Sozen, M. A., "Experimental Study of Reinforced Concrete Assemblies under Column Removal Scenario," *ACI Structural Journal*, V. 111, No. 4, July-Aug. 2014, pp. 881-892. doi: 10.14359/51686739

7. Qian, K., and Li, B., "Slab Effects on the Response of Reinforced Concrete Substructures after Loss of Corner Column," *ACI Structural Journal*, V. 109, No. 6, Nov.-Dec. 2012, pp. 845-855.

8. Xuan Dat, P., and Tan, K. H., "Experimental Study of Beam-Slab Substructures Subjected to a Penultimate-Internal Column Loss," *Engineering Structures*, V. 55, 2013, pp. 2-15. doi: 10.1016/j.engstruct.2013.03.026

9. Ren, P. Q.; Li, Y.; Lu, X. Z.; Guan, H.; and Zhou, Y. L., "Experimental Investigation of Progressive Collapse Resistance of One-Way Reinforced Concrete Beam-Slab Substructures under a Middle-Column-Removal Scenario," *Engineering Structures*, V. 118, July 2016, pp. 28-40. doi: 10.1016/j.engstruct.2016.03.051

10. Qian, K.; Li, B.; and Zhang, Z., "Influence of Multicolumn Removal on the Behavior of RC Floors," *Journal of Structural Engineering*, ASCE, V. 142, No. 5, 2016, p. 04016006 doi: 10.1061/(ASCE)ST.1943-541X.0001461

11. Peng, Z. H.; Orton, S. L.; Liu, J. R.; and Tian, Y., "Experimental Study of Dynamic Progressive Collapse in Flat-Plate Buildings Subjected to Exterior Column Removal," *Journal of Structural Engineering*, ASCE, V. 143, No. 9, 2017, p. 04017125 doi: 10.1061/(ASCE)ST.1943-541X.0001865

12. Qian, K.; Liu, Y.; Yang, T.; and Li, B., "Progressive Collapse Resistance of Post-Tensioned Concrete Beam-Column Sub-assemblages with Un-Bonded Post-Tensioning Strands," *Journal of Structural Engineering*, ASCE, V. 144, No. 1, 2018, p. 04017182 doi: 10.1061/(ASCE)ST.1943-541X.0001940

13. Kim, J., and Choi, H., "Monotonic Loading Tests of RC Beam-Column Subassemblage Strengthened to Prevent Progressive Collapse," *International Journal of Concrete Structures and Materials*, V. 9, No. 4, 2015, pp. 401-413. doi: 10.1007/s40069-015-0119-2

14. GSA, "Progressive Collapse Analysis and Design Guidelines for New Federal Office Buildings and Major Modernization Projects," U.S. General Service Administration, Washington, DC, 2010.

15. UFC 4-023-03, "Design of Building to Resist Progressive Collapse," U.S. Department of Defense, Washington, DC, 2005.

16. ACI Committee 318, "Building Code Requirements for Structural Concrete (ACI 318-14) and Commentary (ACI 318R-14)," American Concrete Institute, Farmington Hills, MI, 2014, 520 pp.

17. Izzuddin, B. A.; Vlassis, A. G.; Elghazouli, A. Y.; and Nethercot, D. A., "Progressive Collapse of Multi-Storey Buildings due to Sudden Column Loss—Part I: Simplified Assessment Framework," *Engineering Structures*, V. 30, No. 5, 2008, pp. 1308-1318. doi: 10.1016/j.engstruct.2007.07.011

18. Tsai, M. H., and Lin, B. H., "Investigation of Progressive Collapse Resistance and Inelastic Response for an Earthquake-Resistant RC Building Subjected to Column Failure," *Engineering Structures*, V. 30, No. 12, 2008, pp. 3619-3628. doi: 10.1016/j.engstruct.2008.05.031

19. Qian, K., and Li, B., "Research Advances in Design of Structures to Resist Progressive Collapse," *Journal of Performance of Constructed Facilities*, V. 29, No. 5, 2015, p. B4014007 doi: 10.1061/(ASCE)CF.1943-5509.0000698

20. Yi, W.; He, Q.; Xiao, Y.; and Kunnath, S. K., "Experimental Study on Progressive Collapse-Resistant Behavior of Reinforced Concrete Frame Structures," *ACI Structural Journal*, V. 105, No. 4, July-Aug. 2008, pp. 433-439.